JBC Papers in Press. Published on December 4, 2002 as Manuscript M212239200

Crystal structures of the BtuF periplasmic binding protein for vitamin B12 suggest a functionally important reduction in protein mobility upon ligand binding.

Nathan K. Karpowich, Hector H. Huang, Paul C. Smith, and John F. Hunt *

Department of Biological Sciences, 702A Fairchild Center, MC2434,
Columbia University, New York, NY 10027, USA.

* Corresponding author: (212)-854-2775 voice; (212)-854-5236 FAX;
hunt@sid.bio.columbia.edu.

Running Title: Crystal structures of *E. coli* BtuF

Keywords: ABC Transporter, vitamin B12, periplasmic binding protein; active transport; protein dynamics; x-ray crystallography.

Version #3: Wednesday, November 27, 2002 @ 8:32 PM.

BtuF is the periplasmic binding protein (PBP) for the vitamin B12 transporter BtuCD, a member of the ATP-binding cassette (ABC) Transporter superfamily of transmembrane pumps. We have determined crystal structures of *E. coli* BtuF in the *apo* state at 3.0 Å resolution and with vitamin B12 bound at 2.0 Å resolution. The structure of BtuF is similar to that of the FhuD and TroA PBP's and is composed of two α/β domains linked by a rigid α-helix. B12 is bound in the "base-on" or vitamin conformation in a wide acidic cleft located between these domains. The C-terminal domain shares structural homology to a B12-binding domain found in a variety of enzymes. The same surface of this domain interacts with opposite surfaces of B12 when comparing ligand-bound structures of BtuF and the homologous enzymes, a change that is probably caused by the obstruction of the face that typically interacts with this domain by the base-on conformation of vitamin B12 bound to BtuF. There is no apparent pseudo-symmetry in the surface properties of the BtuF domains flanking its B12 binding site even though the presumed transport site in the previously-reported crystal structure of BtuCD is located in an intersubunit interface with 2-fold symmetry. Unwinding of an α-helix in the C-terminal domain of BtuF appears to be part of conformational change involving a general increase in the mobility of this domain in the *apo* structure compared to the B12-bound structure. As this helix is located on the surface likely to interact with BtuC, unwinding of the helix upon binding to BtuC could play a role in triggering release of B12 into the transport cavity. Furthermore, the high mobility of this domain in free BtuF could provide an entropic driving force for the subsequent release of BtuF required to complete the transport cycle.

Introduction

The ATP-binding cassette (ABC) transporter superfamily consists of mechanochemically coupled polypeptide complexes in which ATP hydrolysis is coincident with transport of solutes against cellular concentration gradients (1). Members of this family share common structural features that are conserved across the phylogenetic spectrum. The prototypical ABC transporter consists of four subunits, two of which are α-helical transmembrane (TM) domains presumed to determine substrate specificity and trajectory. The other two subunits (the ABC's) are peripherally associated with the cytoplasmic region of the TM domains and mechanically couple ATP hydrolysis to solute translocation (2). In addition, most bacterial importers employ a periplasmic substrate binding protein (PBP) that delivers the ligand to the extracellular gate of the TM domains. ABC transporters have been linked to a number of human diseases, the most notable of which are cystic fibrosis and tumor multidrug resistance (3).

Structures have previously been reported for several PBP's (4), with the maltose binding protein (MBP) being the most widely studied. MBP is composed of two globular domains joined by a hinge region. One maltose molecule binds at the interface of the globular domains. During binding, these domains undergo a substrate-dependent conformational change, rotating approximately 35º about the hinge region (5). Other studies suggest that this conformational change transmits a signal to the TM domains of the maltose transporter promoting ATP-dependent uptake of maltose across the cytoplasmic membrane (6). Most other PBP's have a similar molecular architecture to MBP and presumably function using a similar ligand-induced "clamping" mechanism. PBP's of this kind are subdivided into types (called I and II) based upon the topology of their globular domains (7,8). However, the structure of the TroA Zn^{++} PBP displayed a distinct fold wherein a rigid α-helix connects the two ligand binding domains, suggesting that this sub-class of PBP does not undergo a large scale conformational change of

the same nature as the type I and II PBP's; comparison of free (9) and ligand-bound (10) TroA structures supports this hypothesis.

Vitamin B12 is a large organic cofactor with 93 non-hydrogen atoms that is employed in a diverse array of biochemical reactions ranging from methyl transfers to ribonucleotide reduction (11). B12 is an essential cofactor in all kingdoms of life, and while some bacteria and archaea have evolved the propensity for its synthesis, most prokaryotes and all eukaryotes contain transport systems to import B12 (12). The products of B12 biosynthesis are called coenzyme B12 and have either a 5'-deoxyadenosyl group or a methyl group as the axial ligand of the cobalt atom on the catalytic face of the cofactor. The industrial process used to prepare B12 for human consumption results in the replacement of this axial ligand by a cyano group, leading to a species called cyanocobalamin or vitamin B12 (13). As the biosynthesis of B12 requires approximately 30 enzymatic steps (14), the benefits of importing externally-synthesized molecules are clear. In *E. coli*, the transmembrane transport of B12 is carried out by the Btu (B twelve uptake) system composed of BtuB, an outer membrane TonB-dependent transporter (15), and BtuCDF, an ABC transporter located in the inner membrane. BtuC and BtuD compose respectively the TM domain and the ABC (16), while BtuF is the cognate PBP (17). The crystal structure of the BtuCD integral membrane protein complex has recently been reported (18). We herein present the crystal structures of both vitamin B12-bound and free (*apo*) forms of BtuF.

Experimental Procedures

Protein expression and purification. Pre-BtuF including its N-terminal signal peptide was cloned into pET24 (Novagen), and periplasmic expression of the mature protein was induced for 4 hours at 37˚ C in *E. coli* BL21(DE3) cells. A cleared lysate in 300 mM NaCl, 10 mM imidazole, 10% glycerol, 10 mM DTT, 50 mM potassium phosphate, pH 7.0, was loaded on a Ni-NTA SF (Qiagen) column and eluted with a linear gradient to 250 mM imidazole. Following gel filtration on a Superdex 200 column (Pharmacia) in 100 mM NaCl, 10 mM DTT, 10 mM Tris-Cl, pH 7.5, the protein was concentrated to 10 mg/ml for crystallization. Selenomethionine (SeMet) labeled protein was induced overnight at 37˚ C in B834(DE3) cells grown in M9 minimal media with 50 mg/ml DL-SeMet and the Kao & Michaluk vitamin supplement (Sigma).

Crystallization. Crystals were grown using standard 1:1 hanging-drop vapor diffusion reactions. For the B12 crystals, 5 mM cyanocobalamin (Sigma) was added to the protein stock, and the well solution contained 2.0 M NaCl, 3% ethanol, 100 mM Na-acetate, pH 4.6. Crystals grew to a maximum size of ~200^3 µm over 10 days and were cryoprotected by incubation for 1 hour in the well solution plus 5 mM B12 and 30% glycerol before freezing in liquid propane. *Apo* crystals grew to a maximum size of ~400^3 µm over one week using a well solution containing 30% PEG 4K, 200 mM $(NH_4)Cl$, 100 mM Na-acetate, pH 4.6. They were cryoprotected by incubation for 30 minutes in 40% PEG 4K, 100 mM NH_4Cl, 10**%** glycerol, and 50 mM Na-acetate, pH 4.6.

X-ray data collection and structure determination. Data were collected at NSLS beamline X12C at Brookhaven National Lab using the Brandeis-B4 detector. Multi-wavelength anomalous diffraction datasets were collected in 365˚ sweeps at 0.9785 Å, 0.9787 Å, and 0.9500 Å using 1º oscillations. Data processing and reduction were performed with DENZO and SCALEPACK (19). The 4 Se atom sites in the B12 crystals were determined by SOLVE

(20), and density modification with automated model building was carried out by RESOLVE (21). Density modification with NCS averaging in DM (22) allowed completion of this structure, which was use to solve the *apo* structure by molecular replacement with COMO (23).

Model building, refinement, and molecular graphics. Models were built using O (24) and refined using CNS (25,26) without imposing NCS restraints at any stage. R_{free} sets containing 5% of the reflections were selected at random independently for each crystal form. Refinement comprised iterations of overall anisotropic B-factor refinement, bulk-solvent correction, rigid-body refinement, positional minimization, and individual isotropic B-factor refinement. Residues in the BtuF models are numbered according to their position in the mature protein, *i.e.* after proteolytic cleavage of the 22 residue N-terminal signal peptide in the preprotein. Coordinates and structure factors for the B12-bound and *apo* structures have been deposited in the PDB under accession codes 1N4A and 1N4D, respectively. Molecular interactions were analyzed using the program CONTACT from CCP4 (27) using a cut-off of 3.8 Å for van der Waals contacts and 3.3 Å for H-bonds. Ribbon diagrams were created with MOLSCRIPT (28) or BOBSCRIPT (29) and rendered with Raster3D (30). Surface-rendered images were created with GRASP (31).

Results and Discussion

Overall Protein Structure. BtuF is composed of two globular domains linked by a rigid interdomain α-helix (α6) (Fig. 1). The N-terminal domain I (residues 1-106 of the mature protein) and C-terminal domain II (residues 130-242) possess similar a topology (Fig. 1B) and display 19% sequence identity and a root-mean-square deviation (rmsd) of 4.4 Å for the superposition of 106 Cα atoms (32). As in other types of PBP's, the vitamin B12 transport ligand is bound between the two domains and makes contacts to both.

Domain I is an α/β sandwich composed of a twisted 5-stranded parallel β–sheet with an α–helix connecting each strand (Fig. 1A & 1B). Helix α5 of domain I packs against the interdomain helix α6 to form a partial helical bundle. This domain makes contacts to both the dimethylbenzimidazole (DMB) and propionamide groups on B12 (Figs. 1B & 1C), using residues in helix α1, strand β4, and the loops following strands β2 and β4 (see below). A portion of the topology is conserved between domain I of BtuF and the N-terminal lobes of both type I and II PBP's (Fig. 1B). Specifically, these domains all contain a super-secondary structural element at their N-termini composed of three parallel β–strands linked by two α–helices. Thereafter, both type I and II PBP topologies are divergent from BtuF (7). However, the entirety of domain I of BtuF is structurally similar to the N-terminal domain of FhuD (33), the Fe-siderophore PBP (residues 35-127), and these regions share 20% sequence identity and an rmsd of 2.5 Å for superposition of 101 Cα atoms. This superposition (Fig 2A) reveals an expanded ligand-binding cavity of BtuF relative to FhuD, presumably to accommodate the increased ligand volume of B12 versus gallichrome. Furthermore, BtuF shares the same fold as the TroA Zn^{++}-binding protein (10) both in domain I and also in domain II where their topologies diverge from that of FhuD (Fig. 1B). However, TroA has an additional β-hairpin inserted into domain I, and its mode of ligand recognition and possibly release is distinct from that of BtuF (see below).

Domain II is also an α/β sandwich composed of a 4-stranded parallel β–sheet with connecting α–helices. The C-terminal helix (α11) packs against the interdomain helix (α6) as observed for helix α5 in domain I. Clearly, domain II has diverged from the Fe-siderophore class of PBP's, as the FhuD structure contains a 5-stranded β–sheet with mixed topology (33). However, a DALI (32) search of the PDB revealed that domain II has significant structural homology to the B12-binding domains in methionine synthase (MetE, PDB id 1BMT) (34) and methylmalonyl-CoA mutase (MMCM, PDB id 1REQ) (35), two enzymes that catalyze methyl transfer reactions. These two enzymes share only 9% and 13% sequence identity to domain II of BtuF, respectively. Nonetheless, there is 3.4 Å rmsd for the superposition of 88 Cα's in domain II with residues 583 to 721 in MetE (Fig. 2B) and similar structural homology with MMCM.

Previous studies suggests a common mode of cobalamin binding by this domain. In both MetE and MMCM, the bound B12 is in the "base-off" conformation (Fig. 2B) where the DMB moiety has been displaced as one of the axial ligands of the central cobalt atom by a histidine residue that is conserved in the enzymes but absent in BtuF. This histidine modulates the reactivity of the other axial ligand of the cobalt atom on the opposite "catalytic surface" of the B12 molecule (11). However, B12 is clearly bound to BtuF in the "base-on" conformation in which N2 of DMB remains coordinated to the central cobalt, with the cyanide moiety of cyanocobalamin as the other axial ligand on the opposite face (Figs. 2B & 3A). Presumably, this conformation was selected in order to preserve the co-factor in an unreactive conformation until delivered to the appropriate intracellular enzymes, as dissociation of the DMB is a key step in the activation of coenzyme B12 (11). Probably as a result of this conformational difference in B12, domain II of BtuF binds the opposite surface of the ligand as MetE and MMCM. Domain II in BtuF contacts the catalytic surface of B12 (with bound cyanide), while the equivalent domain in the structural homologues contacts the opposite surface of B12 where the DMB has been displaced by the conserved histidine residue. In all cases, the homologous domains interact with a flat surface of

the B12 ring (Fig. 2B). The reversal of binding geometry in BtuF may be caused by obstruction of the face that typically interacts with this domain by the DMB moiety in the base-on conformation.

Geometry of Vitamin B12 Binding. The highly conserved (Fig. 3B) B12 binding site in BtuF is strongly acidic (Fig. 3C) in spite of the fact that the protein molecule as a whole is slightly basic (pI ≈ 7.9). The DMB-binding surface of B12 interacts exclusively with residues in domain I in BtuF, while the catalytic surface interacts exclusively with domain II (Fig. 3A). In contrast to the type I and II PBP's and TroA, there is significant solvent-exposure of the bound ligand, as also observed in the FhuD complex with gallichrome (33). Nonetheless, approximately 820 $Å^2$ of the solvent-accessible surface area of the vitamin B12 is buried in the complex, corresponding to 62% of the total. Eleven residues in BtuF (shaded pink in Fig. 1C) make direct contacts to the bound vitamin B12 (Figs. 3A and 4B). In addition, 6 residues (shaded green in Fig. 1C) mediate water-mediated hydrogen bonds (H-bonds) to the ligand that are conserved between the two NCS-related BtuF monomers in the crystal structure (see the green spheres in Fig. 3A).

A total of 6 residues in domain I make 50 direct contacts to B12 (Figs. 3A and 4B). The backbone oxygen of ala-10 in helix α1 forms an H-bond to the propionamide nitrogen of Ring A in the corrin, while the sidechains of ser-8 and pro-9 in the same helix make van der Waals contacts to other atoms in the same propionamide group. The sidechain of the phylogenetically-invariant residue tyr-28 in strand β2 makes an H-bond to the propionamide oxygen of Ring B, while the sidechain of the phylogenetically-invariant residue trp-63 in strand β4 makes van der Waals contacts to the DMB group. The carbonyl oxygen of the highly conserved residue gly-65 following strand β4 contacts the sugar group of the nucleotide.

A total of 5 residues in domain II make 39 direct contacts to B12 (Figs. 3A and 4B). Four of these residues interact with the propionamide sidechain of Ring D (the sidechains of trp-174 after strand β7, ser-219 in strand β9, and asp-220 and arg-224 in helix α10). Finally, the side chain of glu-223 makes van der Waals contacts to the cyanide group of B12.

The relatively small number of direct atomic contacts between BtuF and vitamin B12 (89 total) stands in contrast to situation observed in vitamin B12-utilizing enzymes. Both methionine synthase (34) and MMCM (35) make over 150 direct contacts to the ligand. BtuF has presumably adapted to make fewer contacts because it must release the ligand to the transporter in response to a relatively small conformational change (see below), while the B12-utilizing enzymes will ideally permanently immobilize the cofactor in a specific geometry. In addition, as most of the contacts are to the periphery of the B12 molecule, *e.g.* the propionamide groups, it is likely that bacteria have evolved the ability to transport cobalamin variants with different axial ligands including 5'-deoxyadenosine.

Conformational Consequences of B12 Binding and Release. Crystal structures were obtained of BtuF both in the presence and absence of the vitamin B12 ligand (Table I and Fig. 4). Both the B12-bound and *apo* crystals contain two BtuF molecules related by non-crystallographic symmetry (NCS) in the asymmetric units of their respective lattices. However, the refinements were performed without imposing any NCS restraints so that the conformations of the two different molecules in each lattice were determined independently. Although the protein molecules in the B12-bound crystal have somewhat similar crystal packing environments and therefore cannot be considered to be completely independent, the molecules in the *apo* crystal have distinct packing environments (Fig. 4B and additional data not shown) and therefore represent two independent views of the conformation of *apo* BtuF that present a consistent picture of the structural consequences of B12 release.

In Fig. 4A, the B12-bound and *apo* molecules are aligned by least-squares superposition of their N-terminal domains. As expected, a large conformational change of the type observed in MBP does not occur as it is sterically prohibited by the rigidity of the interdomain helix α6. However, both *apo* molecules show a rigid body rotation about residue pro-105 at the N-terminus of the interdomain helix, leading to a net displacement of both this helix and domain II compared to the B12-bound structure (Fig. 4A). The magnitude of this rotation is larger in the "B" molecule (*Apo*-B) than the "A" molecule (*Apo*-A), but a similar trajectory of movement is observed in both. In *Apo*-B, the interdomain helix appears to rotate ~10˚ upward upon ligand release, causing helix α8 and strand β9 in domain II to move slightly outward from the B12-binding site. The movement of these secondary structural elements leads to a modest ~1 Å expansion of the ligand-binding cavity (Fig. 4A) that is likely to facilitate ligand exchange. The residue experiencing the largest displacement is pro-132 at the C-terminus of the interdomain helix, which moves ~6 Å in *Apo*-B. This global conformational change is consistently observed in both *apo* BtuF molecules and contrasts with the local change observed in the *apo* structure of TroA (7,8), where the release of Zn^{++} results in an ~1 Å net movement of the two domains towards one another without any obvious conformational changes in peripheral regions.

Comparing the protein structures within the individual domains, the equilibrium conformation of domain I is tightly conserved in both of the *apo* BtuF molecules compared to the B12-bound molecules (Fig. 4A). The backbone B-factors in this domain are also very similar in the *apo* structures and B12-bound structures, except for a local elevation at two sites in the *apo* structures corresponding to protein loops that directly contact B12 when it is bound (Fig. 4B).

In contrast, substantially larger differences are consistently observed in both the equilibrium conformation and backbone B-factors in domain II in the two NCS-related molecules in the *apo* structure (Fig. 4). The backbone B-factors are elevated throughout the entirety of domain II in

the *apo* molecules (Fig. 4B), indicating a global increase in the mobility of domain II upon ligand release. These high B-factors lead to the presence of weak electron density at the corresponding sites in the protein structure. The density is so weak in domain II of the *Apo*-B molecule that it was not possible to interpret the conformation of residues 195-211. Although the corresponding region could be interpreted in the *Apo*-A molecule, it has the highest backbone B-factors in this molecule (Fig. 4B). The least mobile regions in domain II of the *apo* molecules (ß6, α10, and α11) are those in closest proximity to the interdomain helix, so the entire domain would appear to pivot around this point of attachment. However, there also seems to be an increase in the internal mobility of this domain in the absence of B12 as differences in its equilibrium conformation are observed in both *apo* molecules in the regions with high backbone B-factors (Fig. 4A). The largest conformational change occurs in the region of BtuF that has the highest B-factors in the *Apo-A* molecule (and was uninterpretable in the *Apo-B* molecule) and involves the unfolding of both termini of helix α9 in the absence of ligand (Fig 4B). The relatively remote location of these conformational changes compared to the ligand-binding site reinforces the inference that they are coupled to a general increase in the flexibility / mobility of domain II.

The differences in the equilibrium conformation in domain II in the *apo* structures occur near the surface expected to interact with the BtuCD transporter (lower right in Fig. 4A) and are thus likely to inhibit the gratuitous binding of *apo* BtuF to the transporter. Moreover, the consistent increase in the mobility of domain II observed in both of the independently-observed NCS-related *apo* molecules suggest that the conformational entropy of domain II increases after the release of B12 into the transmembrane gate, and this effect could help promote dissociation and recycling of *apo* BtuF (36).

Structural Aspects of BtuF-Mediated Transmembrane Transport. The BtuCD structure (18) contains a B12-sized cavity in the transmembrane region near the periplasmic surface of the transporter at the interface between a pair of BtuC subunits related by 2-fold symmetry. However, computational analyses show that this cavity is sealed from the periplasm (yellow surface in Fig. 4 of reference (18)) indicating that a large conformational change must take place in the BtuC domains upon BtuF-mediated delivery of B12. This delivery process is likely to involve stable binding of BtuF to the transmembrane BtuC subunit based on the results observed with other PBP-dependent bacterial ABC transporters (37). Given the 2-fold symmetry of the BtuC subunits flanking the putative B12-binding site in the transporter, BtuF might be expected to exhibit 2-fold pseudo-symmetry in the regions flanking its B12 binding site. However, detailed examination of the surface features show no detectable symmetry in hydrophobicity (not shown), electrostatic potential (Fig. 3C), or sequence conservation (Fig. 3B) in the 2 lobes of BtuF. While the back surface of the molecule on the opposite face from its B12-binding site shows the lowest level of sequence conservation (not shown), relatively strong conservation is observed on the surfaces surrounding the B12-binding site (Fig. 3B). However, even stronger conservation is observed at the periphery of the BtuF molecule on the surface of domain I furthest away from the B12 ligand (on the far left as shown in Fig. 3B), suggesting that this region that is relatively remote from the B12-binding site might interact directly with BtuC. Future studies will be required to determine how the asymmetrical vitamin B12 and BtuF molecules bind to the symmetrical BtuCD complex during the active transport reaction.

Acknowledgements. The authors would like to thank Anand Saxena and Sal Sclafani of the NSLS for assistance with data collection and Gerwald Jogl for helpful discussions. This work was supported by grants from the March of Dimes and Cystic Fibrosis Foundation to JFH and by the NIH Protein Structure Initiative grant to the Northeast Structural Genomics Consortium. NKK was supported by a predoctoral training grant in biophysics from the NIH.

References

1. Higgins, C. F. (1992) *Ann. Rev. of Cell Bio.* **8**, 67-113

2. Smith, P. C., Karpowich, N., Moody, J., Millen, L., Rosen, J., Thomas, P. J., and Hunt, J. F. (2002) *Mol. Cell* **10**, 139-149

3. Senior, A. E., and Gadsby, D. C. (1997) *Semin. Cancer Biol.* **8**, 143-150

4. Quiocho, F. A., Wilson, D. K., and Vyas, N. K. (1989) *Nature* **340**, 404-407

5. Sharff, A. J., Rodseth, L. E., Spurlino, J. C., and Quiocho, F. A. (1992) *Biochemistry* **31**, 10657-10663.

6. Chen, J., Sharma, S., Quiocho, F. A., and Davidson, A. L. (2001) *Proc. Natl. Acad. Sci. U S A* **98**, 1525-1530

7. Spurlino, J. C., Lu, G. Y., and Quiocho, F. A. (1991) *J. Biol. Chem.* **266**, 5202-5219

8. Newcomer, M. E., Gilliland, G. L., and Quiocho, F. A. (1981) *J. Biol. Chem.* **256**, 13213-13217

9. Lee, Y. H., Dorwart, M. R., Hazlett, K. R., Deka, R. K., Norgard, M. V., Radolf, J. D., and Hasemann, C. A. (2002) *J. Bacteriol.* **184**, 2300-2304

10. Lee, Y. H., Deka, R. K., Norgard, M. V., Radolf, J. D., and Hasemann, C. A. (1999) *Nat. Struct. Biol.* **6**, 628-633

11. Ludwig, M. L., and Matthews, R. G. (1997) *Annu. Rev. Biochem.* **66**, 269-313

12. Warren, M. J., Raux, E., Schubert, H. L., and Escalante-Semerena, J. C. (2002) *Nat. Prod. Rep.* **19**, 390-412

13. Martens, J. H., Barg, H., Warren, M. J., and Jahn, D. (2002) *Appl. Microbiol. Biotechnol.* **58**, 275-285

14. Raux, E., Schubert, H. L., and Warren, M. J. (2000) *Cell Mol. Life Sci.* **57**, 1880-1893

15. Cadieux, N., and Kadner, R. J. (1999) *Proc. Natl. Acad. Sci. U S A* **96**, 10673-10678

16. Bassford, P. J., Jr., and Kadner, R. J. (1977) *J. Bacteriol.* **132**, 796-805

17. Cadieux, N., Bradbeer, C., Reeger-Schneider, E., Koster, W., Mohanty, A. K., Wiener, M. C., and Kadner, R. J. (2002) *J. Bacteriol.* **184**, 706-717

18. Locher, K. P., Lee, A. T., and Rees, D. C. (2002) *Science* **296**, 1091-1098

19. Otwinowski, Z., and Minor, W. (1997) *Methods Enzymol.* **276**, 307-326

20. Terwilliger, T. C., and Berendzen, J. (1999) *Acta Crystallogr. D Biol. Crystallogr.* **55**, 849-861

21. Terwilliger, T. C. (2001) *Acta Crystallogr. D Biol. Crystallogr.* **57**, 1755-1762

22. Cowtan, K., and Main, P. (1998) *Acta Crystallogr. D Biol. Crystallogr.* **54**, 487-493

23. Jogl, G., Tao, X., Xu, Y., and Tong, L. (2001) *Acta Crystallogr. D Biol. Crystallogr.* **57**, 1127-1134

24. Jones, T. A., Zou, J.-Y., Cowan, S. W., and Kjeldgaard, M. (1991) *Acta Crystallogr.* **A47**, 110-119

25. Brunger, A. T., Adams, P. D., Clore, G. M., DeLano, W. L., Gros, P., Grosse-Kunstleve, R. W., Jiang, J. S., Kuszewski, J., Nilges, M., Pannu, N. S., Read, R. J., Rice, L. M., Simonson, T., and Warren, G. L. (1998) *Acta Crystallogr. D. Biol. Crystallogr.* **54**, 905-921

26. Engh, R. A., and Huber, R. (1991) *Acta Crystallogr.* **A47**, 392-400

27. Collaborative Computational Project, N. (1994) *Acta Crystallogr. D Biol. Crystallogr.* **50**, 760-763

28. Kraulis, P. J. (1991) *J. Appl. Crystallogr.* **24**, 946-950

29. Esnouf, R. M. (1999) *Acta Crystallogr. D. Biol. Crystallogr.* **55**, 938-940

30. Merritt, E. A., and Bacon, D. J. (1997) *Methods Enzymol.* **277**, 505-524

31. Nicholls, A., Sharp, K. A., and Honig, B. (1991) *Proteins* **11**, 281-296

32. Holm, L., and Sander, C. (1995) *Trends. Biochem. Sci.* **20**, 478-480

33. Clarke, T. E., Ku, S. Y., Dougan, D. R., Vogel, H. J., and Tari, L. W. (2000) *Nat. Struct. Biol.* **7**, 287-291

34. Drennan, C. L., Huang, S., Drummond, J. T., Matthews, R. G., and Ludwig, M. L. (1994) *Science* **266**, 1669-1674

35. Mancia, F., Keep, N. H., Nakagawa, A., Leadlay, P. F., McSweeney, S., Rasmussen, B., Bosecke, P., Diat, O., and Evans, P. R. (1996) *Structure* **4**, 339-350

36. Landry, S. J., Taher, A., Georgopoulos, C., and van der Vies, S. M. (1996) *Proc.Nat.Acad.Sci.U.S.A.* **93**, 11622-11627

37. Wolf, A., Lee, K. C., Kirsch, J. F., and Ames, G. F. (1996) *J. Biol. Chem.* **271**, 21243-21250

38. Drenth, J. (1994). Principles of Protein X-ray Crystallography., Springer-Verlag, New York

39. Laskowski, R. A., MacArthur, M. W., Moss, D. S., and Thornton, J. M. (1993) *J. Appl. Crystallogr.* **26**, 283-291

40. Wilmot, C. M., and Thornton, J. M. (1990) *Protein Eng.* **3**, 479-493

Table I. *E. coli* BtuF refinement statistics.

	B12-bound	*Apo*	
Crystal Parameters:			
Space group	$P2_12_12$	$C222_1$	
Cell constants at 100 K	132, 92, 45 Å	56, 84, 209 Å	(90˚, 90, 90˚)
Data quality:			
Resolution	20.0 – 2.0 Å	20.0-3.0Å	
R_{sym}	5.6%	7.1%	($I \geq -3\sigma_I$ for observations)
Mean redundancy	4.5	5.6	
Completeness	98.7%	99.9%	(All measured)
	91.9%	83.8%	($I \geq \sigma_I$ after merging)
Mean I/σ_I	24.1	23.6	
Residuals ($F \geq 2\sigma_f$):			
R_{free}	26.2%	29.8%	
R_{work}	21.4%	23.6%	
Model quality:			
R.M.S. bond lengths	0.006 Å	0.008Å	
R.M.S. bond angles	1.3˚	1.3˚	
Ramachandran plot	91.2%	77.2%	core
	8.5%	18.9%	allowed
	0.2%	2.0%	generously allowed
	0.0%	2.0%	disallowed
Model contents:			
Protein residues	244 + 244	244 + 227	
B12 ligands	2	0	
Water molecules	540	0	

Standard definitions were used for all parameters (38). For the B12-bound structure, the value of $\langle I \rangle / \langle \sigma_I \rangle$ was 3.6 in the limiting resolution shell, which was 70% complete for all measured reflections and 49% complete for reflections with $I \geq 2\sigma_I$. For the *apo* structure, the value of $\langle I \rangle / \langle \sigma_I \rangle$ was 3.8 in the limiting resolution shell, which was 71% complete for all measured

reflections and 43% complete for reflections with $I \geq 2\sigma_I$. Coordinates and structure factors for the B12-bound and *apo* structures have been deposited in the PDB under accession codes 1N4A and 1N4D, respectively. The refinement statistics come from CNS, and the Ramachandran analysis was performed with PROCHECK (39).

Figure Legends

Figure 1. Structure of *E. coli* BtuF bound to Vitamin B12. (A) Ribbon diagram of the BtuF•B12 structure color-coded by domain organization, with domain I colored cyan, domain II tan, and the interdomain helix (α6) green. Vitamin B12 is represented as a space-filling model with carbon atoms colored black, nitrogens blue, oxygens red, and phosphorus magenta. **(B)** Topology diagram of BtuF colored as in panel A with arrows representing β-strands and cylinders representing α-helices. **(C)** Sequence alignment of BtuF's (from *E. coli*, *S. typhimurium*, *V. cholorae*, *Y. pestis*, and *R. saloniricum*) and structural homologues FhuD, TroA, the B12-binding domain of methionine synthase (1BMT), and malonyl-CoA mutase (1REQ). Residues that contact B12 directly are colored pink, while residues that make water-mediated contacts are colored lime. Pink asterixes indicate residues that H-bond directly to B12. The classification of well-ordered β-turns (40) is indicated above the structural schematic.

Figure 2. Structural homologues of BtuF. (A) Stereo pair of the structural alignment of the N-terminal domains of BtuF and *E. coli* FhuD bound to gallichrome (PBD id 1EFD). BtuF is colored by domain as above and vitamin B12 is shown in ball-and stick representation and colored magenta. FhuD is colored gold with the bound gallichrome shown in bright green. **(B)** Stereo pair of the structural alignment of Domain II of BtuF with the B12-binding domain of *E. coli* methionine synthase (MetE, PDB id 1BMT). The corrin ring and DMB of B12 are colored brown and red, respectively. MetE is colored blue with the corrin ring and DMB of its bound B12 colored aqua and cyan, respectively.

Figure 3. Structure of the Vitamin B12 binding site of BtuF. (A) Stereo pair of the B12 binding site of BtuF colored as in Fig. 1A, with conserved waters represented as green spheres. The side chains of relevant residues are depicted in ball-and-stick representation colored by domain with associated nitrogen and oxygen atoms blue and red, respectively. Direct and water-

mediated H-bonds are represented by red and green dotted lines, respectively. **(B)** Surface representation of the likely BtuCD-interacting face of BtuF color-ramped according to sequence conservation, with white indicating no conservation and burgundy indicating 100% conservation in the 5 known BtuF's. **(C)** Surface representation of the same face of BtuF color-ramped according to electrostatic potential, with red indicating negative potential, blue indicating positive potential, and fully-saturated colors indicating potential $\geq \pm 5$ kT (assuming an ionic strength of 100 mM).

Figure 4. Conformational changes associated with B12 binding. **(A)** Stereo pair of the two *apo* and two B12-bound molecules aligned by a superposition of their N-terminal domains. The B12-bound molecules are represented as gray semi-transparent worms. The *apo* molecules are color-ramped by main chain B-factors with molecule A going from blue to red and molecule B from cyan to yellow for B-factors from 25-110 $Å^2$. **(B)** The lowest panel shows the average main-chain B-factors while the upper panels show the number of atomic contacts made by each residue in each molecule either to the bound B12 (pink) or to the adjacent protein molecules in the crystal lattice (colored consistently with the traces in the lowest panel).

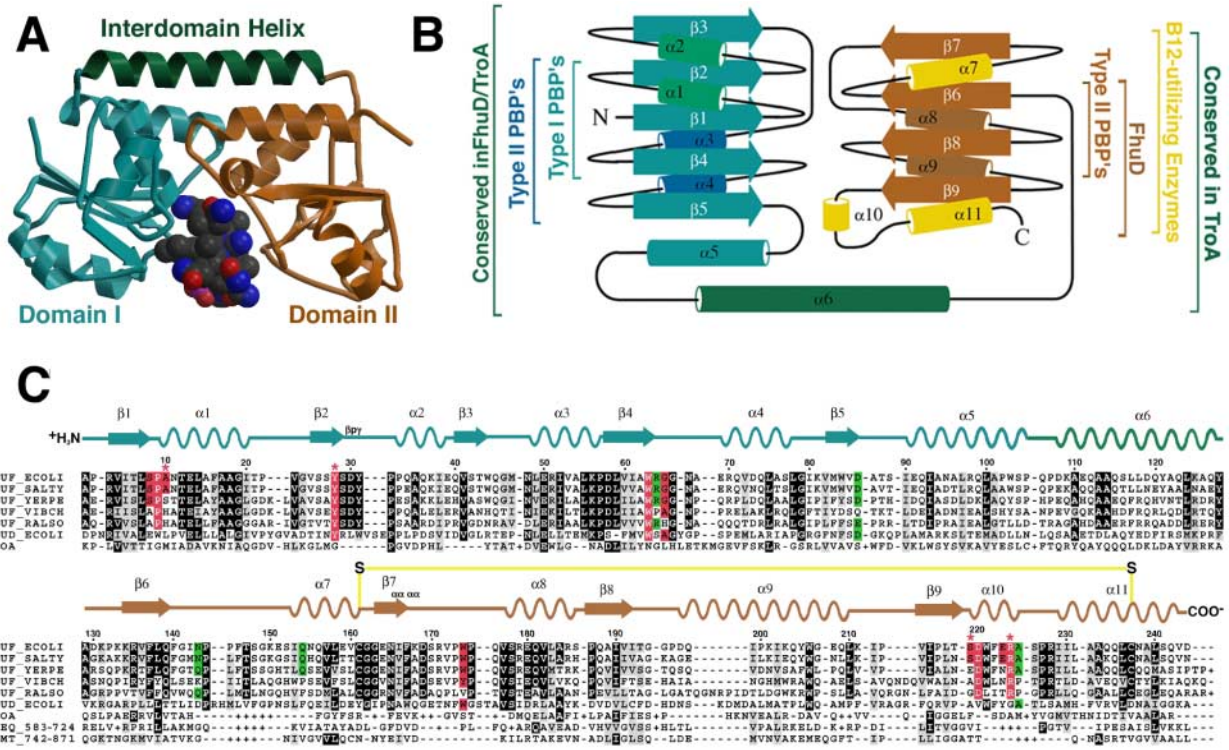

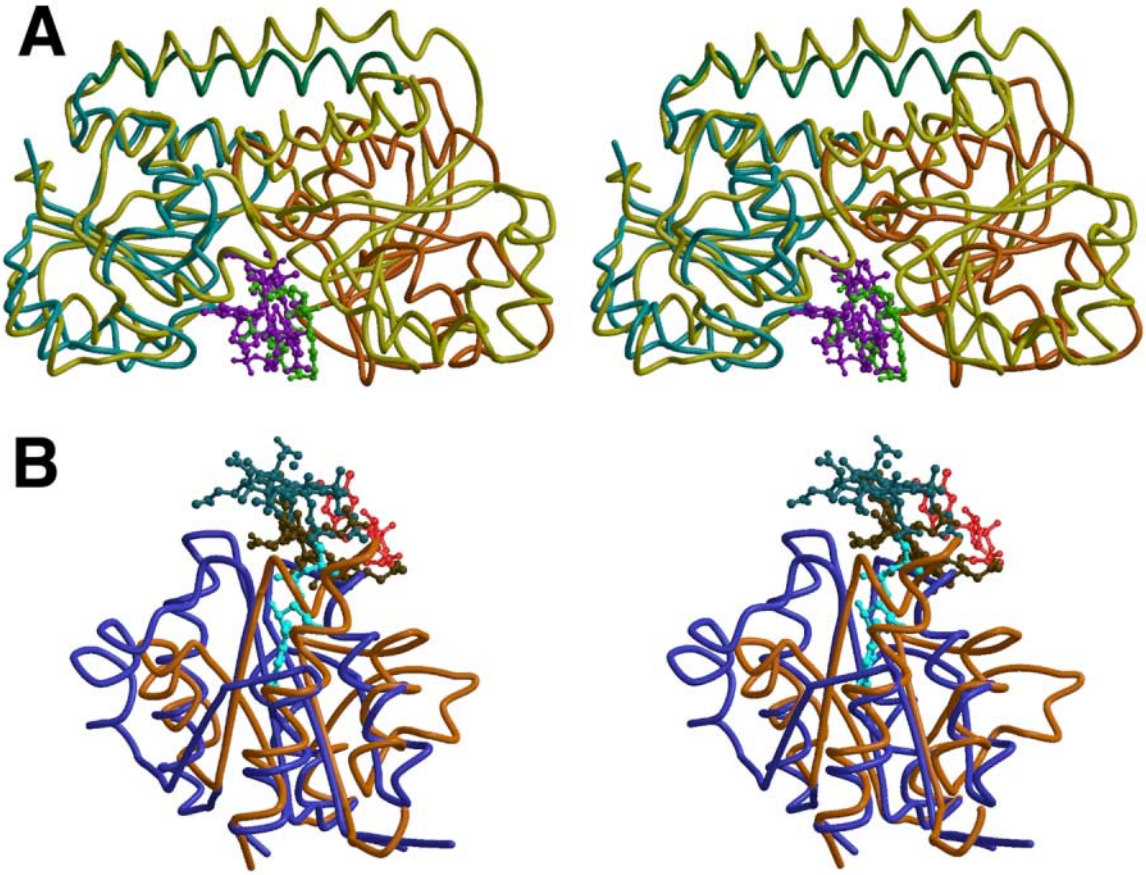

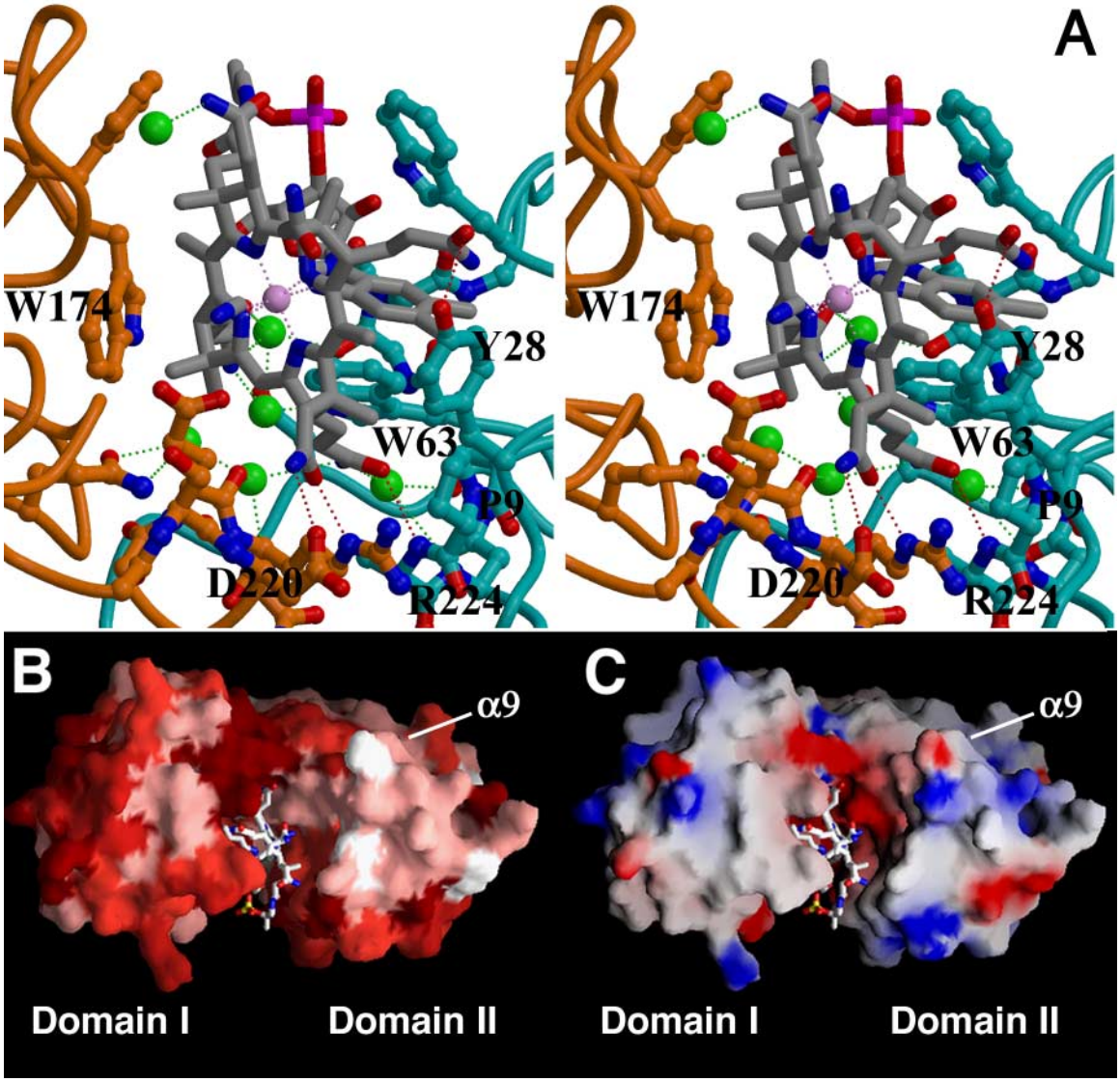

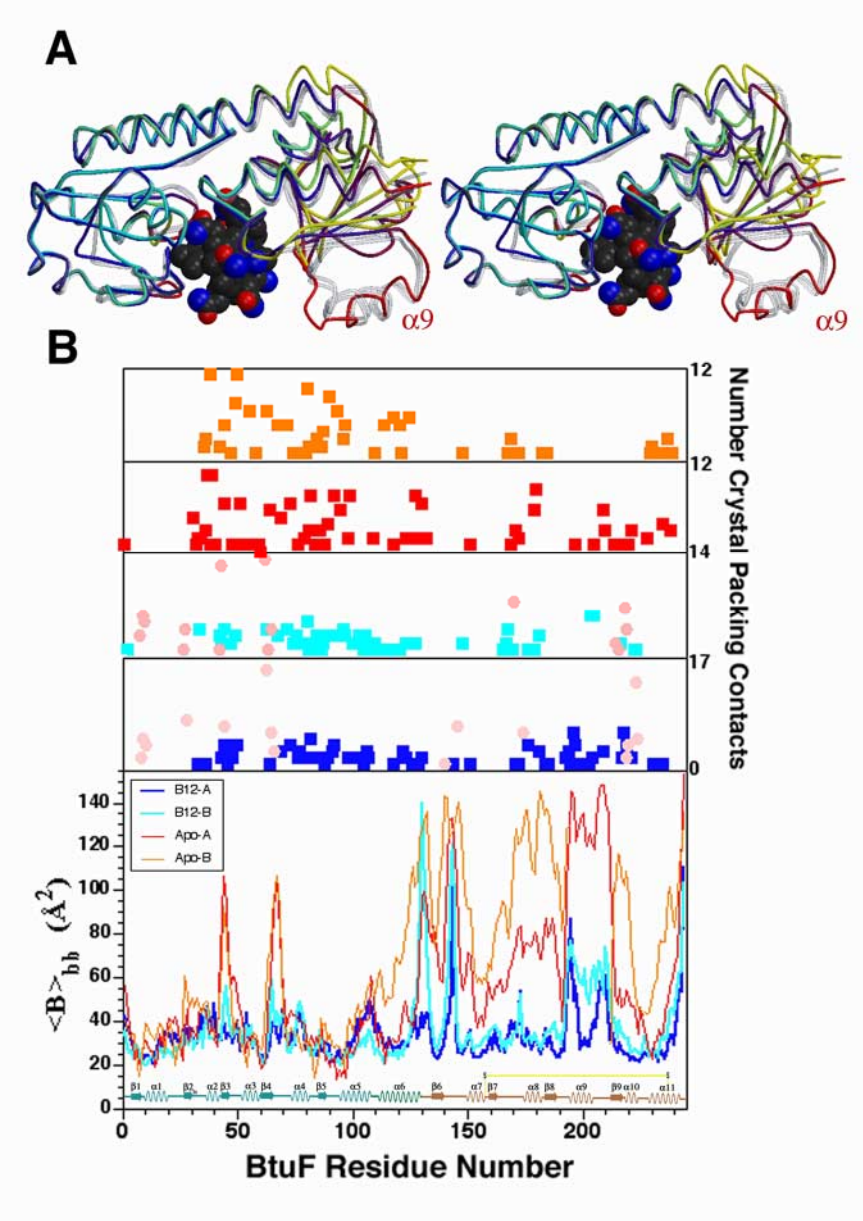

Crystal structures of the BtuF periplasmic binding protein for vitamin B12 suggest a functionally important reduction in protein mobility upon ligand binding

Nathan K. Karpowich, Hector H. Huang, Paul C. Smith and John F. Hunt

J. Biol. Chem. published online December 4, 2002
